Proceedings of the 9th International Symposium on
Dynamics and Control of Process Systems (DYCOPS 2010),
Leuven, Belgium, July 5-7, 2010
Mayuresh Kothare, Moses Tade, Alain Vande Wouwer, Ilse Smets (Eds.)

Forward and inverse integration of population balance equations with size-dependent growth rate

Naim Bajcinca *

* *Max Planck Institute for Dynamics of Complex Technical Systems, Sandtorstr. 1, D-39106 Magdeburg, Germany (e-mail: bajcinca@mpi-magdeburg.mpg.de)*

Abstract: A method for forward and inverse integration of a class of population balance equations with a size-dependent growth rate is contributed in this article. A unique differential transformation of the independent time and internal coordinates is introduced, leading to straight line characteristics with constant values for the density function. The evolution of the density function is then given by transporting the initial and boundary conditions. For the integration of the temporal behavior of the boundary conditions, a generalization of the standard method of moments is introduced, resulting in integro-differential equations involving convolution integrals. The solution to the inverse integration problem involves a pre-computation of given correlation/convolution integrals. The usability of the method is illustrated in a case study of a batch crystallization process with size-dependent growth rate kinetics. The proposed method is compared to a high resolution finite volume scheme using a numerical example.

Keywords: Population balance equation, size-dependent growth rate, method of moments, method of characteristics, simulation, dynamic inversion, batch crystallization processes

1. INTRODUCTION & OUTLINE

Particulate processes are conveniently modeled by a partial differential equation (PDE), designated as the *population balance equation* (PBE), see Randolph and Larson (1988), Ramkrishna (2000). The population balance equation expresses the balance of the number of particles in an infinitesimal particle length interval according to

$$\frac{\partial f}{\partial t} + \frac{\partial (Gf)}{\partial \ell} = 0,\ \ell > 0,\ t > 0 \tag{1}$$

$$f_{\text{b.c.}}(t) \triangleq f(t,0) = \frac{B}{G}(t),\ t \geq 0 \tag{2}$$

$$f_{\text{i.c.}}(\ell) \triangleq f(0,\ell) = f_0(\ell),\ \ell \geq 0, \tag{3}$$

where each particle is associated the internal coordinate ℓ, commonly referred to as the *size* of the particle. The function $f = f(t,\ell)$ represents the *population density function* or *particle size distribution*, defined as the number density of particles per unit length. The underlying population entities may be crystals, droplets, molecules, cells, clouds etc. $f_0(\ell)$ stands for the given initial conditions, *e.g.* seed crystal distribution in a batch crystallization process. The variable G represents the growth rate of the particle size, which, in general, is a time- and size-dependent function, *i.e.* $G = G(t,\ell)$. The birth rate term $B = B(t)$ counts the number of created particles at $\ell = 0$ in a unit time, and hence it impacts the boundary condition (2). In general, additional creation/depletion rate terms modeling diverse phenomena, such as aggregation, agglomeration, breakage, material flux, etc, are included in the right-hand side of the equation (1), thus resulting in an inhomogenous PDE structure. Moreover, *e.g.* in dispersive systems, the PBE in (1) is coupled to additional transfer equations (for mass, momentum, energy, species, etc) providing a feedback to (1). PBE systems including such a coupling are of main concern here.

Computation of the density function $f = f(t,\ell)$ for given initial and operating conditions in (1-3) is referred to as the *forward integration* or *simulation* problem in this manuscript. An accurate integration of a population density function can be challenging in that the distribution may extend over orders of magnitude in both, size and time, and changes in the distribution can be very sharp. This has been an impetus to the development of a variety of numerical integration schemes, including the method of moments, the method of characteristics, finite difference schemes (discrete population balances), recent high-resolution finite volume schemes, etc. As opposed to the numerical discretization schemes, which are developed for a general-purposed use at the price of numerical diffusion and dispersion, the method of characteristics and the method of moments are highly accurate and are efficiently solved, but apply to a rather limited class of problems; for details refer to *e.g.* Braatz (2002). The method of characteristics tempts to identify the characteristic curves in the (t,ℓ)-plane, where the PDE (1) converts to an ODE. The method of moments involves the Mellin integral transform as the definition for the moments of the density function $f = f(t,\ell)$, leading to a closed system of ODEs. However, in a more complex setting, in particular, in the case of size-dependent growth rate, *i.e.* $G = G(t,\ell)$, the method of moments may be afflicted with the violation of the closure condition.

Rather than constructing closure conditions, such as by the quadrature method of moments from McGraw (1997), in this paper, a direct integration scheme (*i.e.* without loss

Copyright held by the International Federation of Automatic Control

of accuracy, since no integral approximations employed) involving the method of characteristics and a generalization of the method of moments is presented. A suitable differential coordinate transformation $(t, \ell) \to (\tau, \lambda)$ is first introduced in (1) to transform it into a transport equation with a unity growth rate (see Section 2)

$$\frac{\partial \tilde{f}}{\partial \tau} + \frac{\partial \tilde{f}}{\partial \lambda} = 0, \ \lambda > 0, \ \tau > 0 \tag{4}$$

$$\tilde{f}_{\text{b.c.}}(\tau) \triangleq \tilde{f}(\tau, 0) = \frac{\tilde{B}}{\tilde{G}_0}(\tau), \ \tau \geq 0 \tag{5}$$

$$\tilde{f}_{\text{i.c.}}(\lambda) \triangleq \tilde{f}(0, \lambda) = \tilde{f}_0(\lambda), \ \lambda \geq 0, \tag{6}$$

where a scaled density function $\tilde{f} = \tilde{f}(\tau, \lambda)$ has been introduced additionally; the precise definitions of the ingredients are given in (11-14). Hereby, the variable separation condition is assumed to hold for the growth rate term

$$G(t, \ell) = \gamma(\ell) G_0(t), \tag{7}$$

which is a commonly encountered assumption in the literature (see Section 3.1).

By making use of the method of characteristics, the solution of equation (4) can be easily expressed in terms of the boundary condition $\tilde{f}(\tau, 0) = \tilde{B}/\tilde{G}_0(\tau)$. To solve for the latter, the method of moments has been utilized in Section 2. It turns out, that the underlying problem can be eventually reformulated as a system of integro-differential equations involving convolution integrals of the boundary condition. In other words, at a specific instant $\tau = \tau_e$, the left-hand side derivatives of the system of differential equations are determined by the history of the boundary conditions in $0 < \tau < \tau_e$, and not just by the current values at τ_e, as in a standard ODE form.

The PBE in (1) often involves external variables which can be used to manipulate the evolution of the density function $\tilde{f}(\tau, \lambda)$. For instance, in a batch crystallizer, the temperature of the cooling medium circulating through the crystallizer is typically used as a control variable. Obviously, the control variable must appear in the boundary condition term $\tilde{B}/\tilde{G}_0(\tau)$ in (5). For a variety of engineering purposes (*e.g.* in process control and optimization) the *inverse integration* or *dynamic inversion* problem, *i.e.* computation of the required profile of the control variable producing a prespecified desired final density function $\tilde{f}_{\text{des}}(\lambda) = \tilde{f}(\tau_e, \lambda)$, $\lambda \in [0, \infty]$ may be crucial. The dynamic inversion problem reduces eventually to solving the algebraic equation $\tilde{f}_{\text{des}}(\tau_e - \tau) = \tilde{B}/\tilde{G}_0(\tau)$ for the control variable in the interval $\tau \in [0, \tau_e]$.

The paper is organized as follows. In Section 2, the underlying differential transformation of the independent time and size coordinates is introduced, and a generalization of the method of moments is devised. In Section 3, the usability of the method is illustrated in a case study of a batch crystallization process with size-dependent growth kinetics. A numerical simulation example is drawn to compare the efficiency of the proposed method to the high resolution finite volume scheme from Koren (1993). In Section 3.3 the feedforward solution scheme to the dynamic inversion problem is presented, and an associated numerical example is inspected. The presented inversion scheme can be interpreted as a generalization of the dynamic inversion method proposed in Vollmer and Raisch (2006), where the (orbital) flatness (*i.e.* analytical invertibility) of a batch crystallization process with *size-independent* growth rate kinetics has been utilized. The useful flatness property is unfortunately lost in the setting with *size-dependent* growth rate kinetics. However, the *invertibility* property is recovered by the work in this paper.

2. MAIN IDEA

Consider the population balance equation in (1-3). Introduce new independent coordinates (τ, λ) by the differential maps

$$\mathrm{d}\tau = G_0(t)\mathrm{d}t, \quad \mathrm{d}\lambda = \frac{\mathrm{d}\ell}{g(\ell)}, \quad \tau(0) = 0, \ \lambda(0) = 0. \tag{8}$$

Since at any point (t, ℓ), $G_0(t) > 0$ and $g(\ell) > 0$ holds, a bijection mapping between the two coordinate frames (t, ℓ) and (τ, λ) exists, *i.e.* the following invertible functions are well defined

$$\tau = \tau(t), \ \lambda = \lambda(\ell), \quad t \geq 0, \ell \geq 0 \tag{9}$$

$$t = t(\tau), \ \ell = \ell(\lambda), \quad \tau \geq 0, \ \lambda \geq 0. \tag{10}$$

The mapping is decoupled in the sense that variables ℓ and t do not interact to τ and λ, respectively. Since the size-independent factor $G_0(t)$ of the growth rate depends on the process evolution, *i.e.* on the evolution of the density function $f(t, \ell)$, the function $\tau = \tau(t)$, *i.e.* its inverse $t = t(\tau)$, have to be computed online. On the other hand, for a given size-dependent growth rate term $\gamma(\ell)$, the equation $\lambda = \lambda(\ell)$, that is, its inverse $\ell = \ell(\lambda)$, can be integrated directly from (8), as shown *e.g.* in Section 3.1 for a particular model.

Applying the differential maps (8) into the original PBE (1-3) leads directly to the transformed PBE equation to (4-6). Thereby, the following settings hold

$$\tilde{f}(\tau, \lambda) \triangleq \gamma(\ell(\lambda)) f(t(\tau), \ell(\lambda)) \tag{11}$$

$$\tilde{B}(\tau) \triangleq B(t(\tau)) \tag{12}$$

$$\tilde{G}_0(\tau) \triangleq G_0(t(\tau)) \tag{13}$$

$$\tilde{f}_0(\lambda) \triangleq g(\ell(\lambda)) f_0(\ell(\lambda)). \tag{14}$$

Equations (8) infers that the lines $\mathrm{d}\ell/\mathrm{d}t = \gamma(\ell) G_0(t) \triangleq G(t, \ell)$ map to

$$\frac{\mathrm{d}\lambda}{\mathrm{d}\tau} = 1 \tag{15}$$

in the (τ, λ)-domain, that is, all particles grow with the same rate equal to unity. It is easy to show, that straight lines with unity slope constitute the characteristics of the PDE (4) in the sense of the method of characteristics. The solution of the (4) along such characteristics reads $\tilde{f}(\tau, \lambda) = \text{const}$, see Fig. 1. This is an important outcome, since the evolution of the density function in (1) is directly expressed in terms of the initial and boundary conditions. Indeed, for a fixed τ, see Fig. 1, the distribution $\tilde{f}(\tau, \lambda)$ reads

$$\tilde{f}(\tau, \lambda) = \begin{cases} \tilde{f}(\tau - \lambda, 0) = \dfrac{\tilde{B}}{\tilde{G}_0}(\tau - \lambda), \ \lambda < \tau \\ \tilde{f}(0, \lambda - \tau) = \ \tilde{f}_0(\lambda - \tau), \ \lambda > \tau. \end{cases} \tag{16}$$

In other words, the integration of the PBE (4) reduces to the computation problem of the temporal evolution of the boundary condition (5) in the τ-domain. Therefore, in the sequel, a generalization of the method of moments is used.

First, notice that the 0th moment of the distribution

Copyright held by the International Federation of Automatic Control

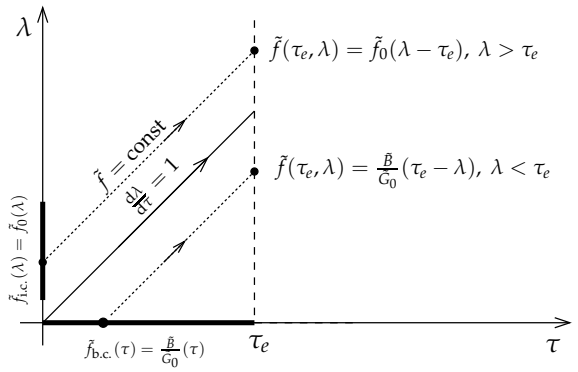

Fig. 1. Characteristic lines ($\mathrm{d}\lambda/\mathrm{d}\tau = 1$) for the PBE (4).

(*i.e.* the number of the crystal particles) is an invariant of the transformation (8) since

$$\int_0^\infty \tilde{f}(\tau,\lambda)\mathrm{d}\lambda = \int_0^\infty f(t,\ell)\mathrm{d}\ell. \tag{17}$$

Application of the 'dot'-operator $\partial/\partial\tau$ on the left-hand side of the equation after usual integral manipulations (*i.e.* substitution of (4) and integration by parts) reveals the ODE

$$\dot{\mu}_0 = \frac{\tilde{B}}{\tilde{G}_0}(\tau). \tag{18}$$

It is further obvious that the analytical expressions for the higher moments $\mu_i = \mu_i(\tau)$ of the distribution function $f(t,\ell)$ in the $(\tau,\lambda)-$domain read

$$\mu_i(\tau) = \int_0^\infty \ell^i(\lambda)\tilde{f}(\tau,\lambda)\mathrm{d}\lambda,\ i = 1,2,\cdots. \tag{19}$$

Differentiation of these integral expressions *w.r.t.* τ does not, however, produce an analytical expression in μ_i. Hence, no closed ODE system can be constructed consisting purely of the moments μ_i of the distribution function $f(t,\ell)$. Instead, one has to introduce the integral moments of the scaled density function $\gamma(\ell)f(t,\ell)$

$$\tilde{\mu}_i(\tau) \triangleq \int_0^\infty \ell^i(\lambda)\tilde{\gamma}(\lambda)\tilde{f}\,(\tau,\lambda)\,\mathrm{d}\lambda,\ i = 1,2,\cdots, \tag{20}$$

where $\tilde{\gamma}(\lambda) = \gamma(\ell(\lambda))$. In fact, it can be checked that the following system of integro-differential equation results

$$\dot{\mu}_0 = \frac{\tilde{B}}{\tilde{G}_0}(\tau), \tag{21}$$

$$\dot{\mu}_i = i\tilde{\mu}_{i-1}(\tau),\ i = 1,2,\cdots. \tag{22}$$

[*Remark:* For size-independent growth rate, *i.e.* $\gamma(\ell) = 1$, $\tilde{\mu}_i = \mu_i$, and a closed ODE system consisting of a chain of integrators, *i.e.* sharing the flatness property, results]. A structural reduction and a better insight into the process dynamics described by (21-22) is gained if the moments μ_i and $\tilde{\mu}_i$ are separated into portion (or partial) moments stemming from the initial and boundary conditions (5) and (6). Indeed, it can be easily checked that

$$\mu_i = \mu_{i,n} + \mu_{i,s},\quad \tilde{\mu}_i = \tilde{\mu}_{i,n} + \tilde{\mu}_{i,s},\quad ,\ i = 1,2,\cdots \tag{23}$$

with

$$\mu_{i,n} \triangleq \int_0^\tau \ell^i(\lambda)\frac{\tilde{B}}{\tilde{G}_0}(\tau-\lambda)\mathrm{d}\lambda, \tag{24}$$

$$\tilde{\mu}_{i,n} \triangleq \int_0^\tau \ell^i(\lambda)\tilde{\gamma}(\lambda)\frac{\tilde{B}}{\tilde{G}_0}(\tau-\lambda)\mathrm{d}\lambda, \tag{25}$$

$$\mu_{i,s} \triangleq \int_0^\infty \ell^i(\lambda)\tilde{f}_0(\tau+\lambda)\mathrm{d}\lambda, \tag{26}$$

$$\tilde{\mu}_{i,s} \triangleq \int_0^\infty \ell^i(\lambda)\tilde{\gamma}(\lambda)\tilde{f}_0(\tau+\lambda)\mathrm{d}\lambda, \tag{27}$$

where, additionally, the transport equations (16) have been substituted, leading to correlation and convolution integral forms. It is clear hereof that partial moments stemming from the initial conditions $\mu_{i,s}$ and $\tilde{\mu}_{i,s}$ are driven by the 'time' τ only, and, thus, can be integrated directly, independently on the process evolution. [*Remark:* This is a generalization of the polynomial dependency of the moments μ_i in τ in the case with a size-independent growth rate, see Bajcinca et al. (2010).]

On the other hand, it is an easy exercise to prove that the form of the net dynamics (22) is inherited by the moments $\mu_{i,n}$ and $\tilde{\mu}_{i,n}$, that is,

$$\dot{\mu}_{0,n} = \frac{\tilde{B}}{\tilde{G}_0}(\tau), \tag{28}$$

$$\dot{\mu}_{i,n} = i\tilde{\mu}_{i-1,n},\ i = 1,2,\cdots. \tag{29}$$

[*Remark*: Eq. (22) holds for the moments $\mu_{i,s}$ and $\tilde{\mu}_{i,s}$, too. In particular, $\dot{\mu}_{0,s} = 0$.] Hence, equations (28-29) represent a reduced version of the moment model in (21-22). The resulting model consists of a system of integro-differential equations, where moment derivatives are driven by appropriate convolution integrals applying on the boundary conditions.

The PBE (1) in dispersive particulate processes is coupled to additional transfer equations for mass, energy, etc. Such equations implicitly impact the driving force for the particle growth, Ramkrishna (2000), by providing a feedback from the net moments μ_i into the input term $\tilde{B}/\tilde{G}_0(\tau)$ in (28). For instance, mass balance law describing the material transfer between the continuous and dispersed phase reads

$$\begin{aligned}\dot{m}_c &= -3\rho k_v \int_0^\infty \ell^2(\lambda)\tilde{\gamma}(\lambda)\tilde{f}(\tau,\lambda)\mathrm{d}\lambda \\ &= -3\rho k_v(\tilde{\mu}_{2,n} + \tilde{\mu}_{2,s}),\quad m_\mathrm{c}(0) = m_0,\end{aligned} \tag{30}$$

i.e.

$$m_\mathrm{c} = m_0 + m_\mathrm{s} - \rho k_v \mu_3, \tag{31}$$

where $m_\mathrm{c} = m_\mathrm{c}(\tau)$ is the mass dispersed in the continuous phase, $m_\mathrm{s} = \rho k_v \mu_{3,s}(0)$ is the initial mass in the dispersed phase, ρ is the particle mass density, and k_v is a volume shape factor, Randolph and Larson (1988). The latter equation reveals the impact of the moment $\tilde{\mu}_{2,s}$, *i.e.* $\mu_{3,s}$ on the process dynamics in the (τ,λ)-domain. In this particular case, the 3rd moment $\mu_{3,n}$ closes the system, due to its feedback to the input term $\tilde{B}/\tilde{G}_0(\tau)$.

To summarize, by this approach, no closure conditions for the method of moments are constructed. Rather, a direct method for the integration of the density function $\tilde{f}(\tau,\lambda)$, that is, $f(t,\ell)$, is obtained, provided that a higher moment, as μ_3 in the latter example, couples to the equation (28), *e.g.* by a transfer equation. The model (28-29) can be integrated numerically, *e.g.* by using standard fixed step solvers.

Copyright held by the International Federation of Automatic Control

3. CASE STUDY: BATCH CRYSTALLIZATION

In this section, the proposed scheme is applied for forward and inverse integration of a batch crystallization process. For the sake of completeness, the standard size-dependent kinetics is first reviewed.

3.1 Process kinetics

A batch crystallizer is made up of a large number of crystal particles immersed in a dispersed phase system (solution), constituted by a continuous liquid medium (solvent, typically water) and dispersed crystalline (solute) entities (molecules or ions), in which mass transfer of the solute from the liquid to a pure solid crystalline phase occurs. The fundamental force for crystallization from the solution arises effectively from the level of supersaturation (S), which is a measure of the difference between the solution concentration (c) and saturation concentration (c_{sat}), see Myerson (2002),

$$S = c/c_{\text{sat}}, \text{ with } c = m_{\text{c}}/(m_{\text{w}} + m_{\text{c}}), \tag{32}$$

where m_{w} is the solvent and m_{c} the solute mass. The latter can be *e.g.* controlled by the temperature (T) using the empirical model

$$c_{\text{sat}} = a_0 + a_1 T + a_2 T^2, \tag{33}$$

where a_0, a_1, and a_2 are positive parameters.

Batch crystallization is usually used for a purposeful growth of rather small seed crystals, which are dipped into a supersaturated solution containing a solute of the same material. In parallel to the growth process, nucleation occurs, *i.e.* solute molecules gather into stable clusters which constitute new nuclei. Within the so-called metastable region, which exists in a moderately supersaturated solution, the nucleation rate B and the growth rate G_0 are driven by the supersaturation level according to

$$B = k_b \left(S-1\right)^b \mu_3, \quad G_0 = k_g \left(S-1\right)^g, \tag{34}$$

where k_g, g, k_b and b are empirical (positive) parameters, too, and μ_3 is the 3rd moment of the density function of the solid phase.

Experimental investigations of different crystallization processes (*e.g.* certain inorganic hydrated salts) demonstrate a size-dependent growth rate of crystal particles. Different models on size-dependent growth rate have been proposed, such as Abegg-Stevens-Larson (abbr. ASL) model, Canning and Randolph (abbr. C-R) model, Bransom model, MJ2/MJ3 models, see Abegg et al. (1968), Myerson (2002). All models fulfill the separation condition (7), *e.g.* ASL-model: $\gamma(\ell) = (1+\alpha\ell)^z, z < 1$, C-R model: $\gamma(\ell) = 1 + \alpha\ell$. For the ASL-model the bijection condition (9) is clearly observed from

$$\lambda(\ell) = \frac{(1+\alpha\ell)^{1-z}}{\alpha(1-z)}, \text{ and } \ell(\lambda) = \frac{1-(\alpha(1-z)\lambda)^{\frac{1}{1-z}}}{\alpha}.$$

3.2 Forward integration

The dynamics of a batch crystallization process can be completely captured by a PBE of the form (1), augmented by the mass-balance law (31), referring to the material transfer from the liquid to the solid phase due to nucleation and crystal growth. Owing to the discussion in Sections 2 and 3.1, one can directly constitute the system of integro-differential equations representing the full model of a batch crystallization process with size-dependent growth kinetics in the (τ, λ)-domain

$$\dot{\mu}_{0,n} = \frac{\tilde{B}}{\tilde{G}_0}(T, \mu_{3,n} + \mu_{3,s}) \tag{35}$$

$$\dot{\mu}_{3,n} = 3\tilde{\mu}_{2,n} \tag{36}$$

$$\dot{t} = \frac{1}{\tilde{G}_0}(T, \mu_{3,n} + \mu_{3,s}), \tag{37}$$

with

$$\tilde{\mu}_{2,n} = \int_0^{\tau} \ell^2(\lambda)\tilde{\gamma}(\lambda)\frac{\tilde{B}}{\tilde{G}_0}(\tau-\lambda)\mathrm{d}\lambda, \tag{38}$$

$$\tilde{\mu}_{3,s} = \int_0^{\infty} \ell^3(\lambda)\tilde{f}_{\text{seed}}(\tau+\lambda)\mathrm{d}\lambda, \tag{39}$$

and $\mu_{0,n}(0) = \mu_{2,n}(0) = 0$. Note that it is convenient to include an ODE for the 'real' time variable t, in order to keep track of certain specifications (*e.g.* process length), which are naturally expressed directly in terms of the the 'real' time t. Moreover, the algebraic equation for the mass-balance (31) is substituted in (32) and (34). Again, $\mu_{3,s}$ is pre-computed by making use of (39) with $\tilde{f}_{\text{seed}}(\lambda) = \tilde{f}_0(\lambda)$ representing the distribution function of the seeded crystal particles. Apart from the temperature $T = T(\tau)$, the 3rd moment $\mu_{3,s} = \mu_{3,s}(\tau)$ plays the role of an input to the resulting simulation scheme.

The precise formulation of the forward integration (*i.e.* simulation) problem in the (τ, λ)-domain reads: for a given initial distribution of seed crystals $\tilde{f}_{\text{seed}}(\lambda)$, *i.e.* for a given evolution of $\mu_{3,s}(\tau)$, and an input temperature profile $T(\tau)$, $\tau \in [0, \tau_e]$, compute the evolution of $\mu_{3,n}(\tau)$ for $\tau \in [0, \tau_e]$. Having solved this problem, the evolution of the boundary condition is computed from

$$\tilde{f}_{\text{b.c.}}(\tau) = \tilde{f}(\tau, 0) = \frac{\tilde{B}}{\tilde{G}_0}(T(\tau), \mu_{3,n}(\tau) + \mu_{3,s}(\tau)). \tag{40}$$

In the t-domain, the moments $\mu_i(t) = \mu_{i,n}(t) + \mu_{i,s}(t), i = 0, 3$, for $t \in [0, t_e]$, where $t_e = t(\tau_e)$, are computed by the composition of the solutions in the τ-domain with the function $\tau = \tau(t)$, *i.e.* the inverse of the solution $t = t(\tau)$ from (37). The distribution function $f = f(t_e, \ell)$, $0 < \ell < \infty$ is, finally, constructed by

$$f(t_e, \ell) = \begin{cases} \tilde{f}_{\text{b.c.}}\left(\tau_e - \lambda(\ell)\right)/\gamma(\ell), & 0 < \ell < \gamma^{-1}(\tau_e) \\ \tilde{f}_{\text{seed}}\left(\lambda(\ell) - \tau_e\right)/\gamma(\ell), & \ell > \gamma^{-1}(\tau_e). \end{cases}$$

3.3 Inverse integration

In the (τ, λ)-domain, the temperature profile can only influence the density function originating from the boundary conditions, *i.e.* from the nucleation. Thus, the precise formulation of the inverse integration problem requires the computation of the input temperature profile $T(\tau)$, $\tau \in [0, \tau_e]$ that produces a desired distribution function

$$\tilde{f}_{\text{des}}(\lambda) = \tilde{f}(\tau_e, \lambda), \quad \lambda \in [0, \tau_e].$$

Due to (16), this is equivalent to setting a desired course for the boundary condition

$$\tilde{f}_{\text{des}}(\tau_e - \tau) = \frac{\tilde{B}}{\tilde{G}_0}\left(T, \mu_{3,n} + \mu_{3,s}\right), \ \tau \in [0, \tau_e]. \tag{41}$$

Copyright held by the International Federation of Automatic Control

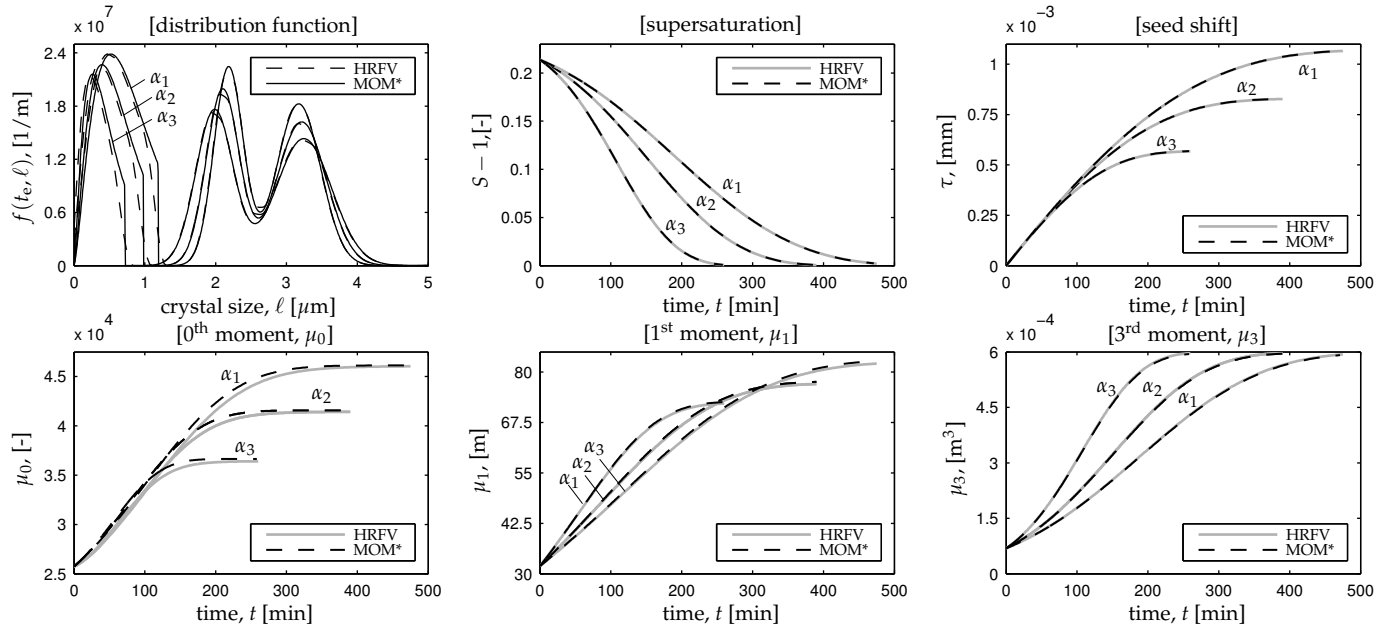

Fig. 2. Simulation numerical results with the high resolution finite volume scheme (HRFV) and the with the proposed method of moments (MOM*). The marks α_1, α_2, and α_3 refer to the α parameter in the C-R model, see Table 1.

Given the inputs $\tilde{f}_{\text{seed}}(\lambda)$ and $\tilde{f}_{\text{des}}(\lambda)$, the temporal evolution of the 3rd moment $\mu_3(\tau) = \mu_{3,n}(\tau) + \mu_{3,s}(\tau)$ is again pre-computed by (39). Hence, the dynamic inversion problem, reduces to solving the algebraic equation (41) for $T = T(\tau)$, $\tau \in [0, \tau_e]$. Note that strictly speaking, the computed profile refers to the set-point temperature for the cooling medium in the crystallizer jacket T_j. But, for the sake of simplicity the ODE for the heat exchange is here ignored.

A specification of the desired shape of the density function $f_{\text{des}}(\ell)$ is naturally set in the (t, ℓ)-domain. But, this can be easily converted to a specification in the (τ, λ)-domain. Indeed, from the shifting of the final seed distribution portion $f_{\text{seed}}(\ell)$ in the desired $f_{\text{des}}(\ell) = f(t_e, \ell)$, the process 'length' τ_e can be directly computed, and using (10), $\tilde{f}_{\text{des}}(\lambda) = \tilde{f}(\tau_e, \lambda)$ is constructed from $f(t_e, \ell)$. The back-mapping of the solution $T = T(\tau)$ in the t-domain is done, as in the simulation scheme, by the composition $T = T(\tau(t))$. Hence, hereby, the ODE (37) for the time t has to be integrated, additionally.

3.4 Numerical example

For validation purposes, two numerical problems concerning the forward and inverse integration of a batch crystallization process with a threonine enantiomer are considered here. In a first numerical example, the simulation results produced by the method proposed in this paper (abbr. MOM*), are compared to those resulting from the high-resolution scheme, introduced in Koren (1993) (abbr. HRFV). Recall that high-resolution schemes are developed to provide a high-order of accuracy while avoiding numerical diffusion and dispersion associated to other finite difference and finite volume schemes, see Qamar et al. (2006), Gunawan et al. (2004). In the second example, numerical results for the dynamic inversion scheme are presented. The problem data, borrowed from Qamar et al. (2006), including the process parameters and the initial conditions are listed in Table 1. Note that C-R model $\gamma(\ell) = 1 + \alpha\ell$ has been utilized for the size-dependent kinetics.

In simulation plots, the crystallization process is driven by a constant temperature $T = 29.5998$ °C, corresponding to $c_{\text{sat}} = 0.0907$. As time progresses, the supersaturation is exhausted ($S \to 1$), that is, the solid-liquid phase system reaches the equilibrium and the crystallization process is completed. This is clearly observed in Fig 2; for a larger parameter α, the process terminates earlier. The predictions of both methods for the 3rd moment μ_3, supersaturation $S - 1$ and τ are nearly identical for different values of size-dependent growth parameter α. However, the final distribution function $f(t_e, \ell)$ reveals major accuracy differences, especially in the portion arising from the nucleation. The differences are further clearly reflected in the predictions for μ_0, and less for μ_1. The inaccuracy of the high resolution scheme is caused by the numerical diffusion, clearly observed about the discontinuity of the density function ($\approx 1[\mu\text{m}]$). [*Remark*: A grid with 300 discretization points in the internal size and time axis has been used]. On the other hand, the proposed scheme predicts an accurate shape with a sharp discontinuity. [*Remark*: The numerical integration of the system (35-37) has been carried out by using the classical fixed-step RK4 solver, involving 300 equal discreatization steps in $[0, \tau_e]$.]

For validation of the dynamic inversion scheme, a reference temperature profile (solid gray plot denoted by 'ref' in Fig 3) is applied to generate the desired profile $f_{\text{des}}(t_e, \ell)$ (solid gray). The latter is then used to compute the required temperature profile (dashed plot denoted by 'inv' in the figure) by the dynamic inversion scheme. The two temperature profiles, and the resulting distribution functions show a perfect match. Additionally, the supersaturation, as an important process variable, of the forward and inverse integration schemes are compared, too.

Copyright held by the International Federation of Automatic Control

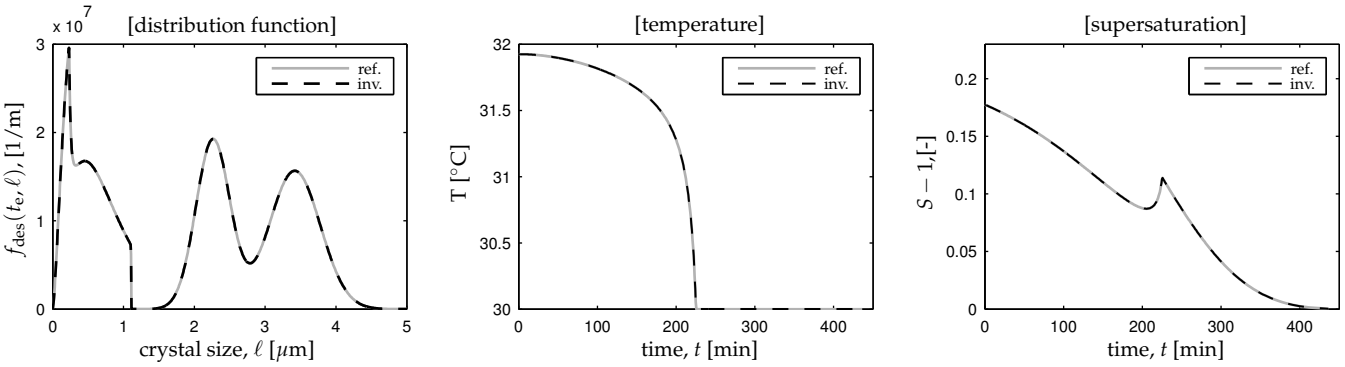

Fig. 3. Numerical results of the dynamic inversion scheme with $\alpha = \alpha_2$, see Table 1.

CONCLUSION

In this manuscript a new method for the forward and inverse integration of the PBE (population balance equation) involving size-dependent growth kinetics is proposed. A unique coordinate transformation has been introduced, leading to straight line characteristics. As a consequence, the forward and inverse integration problems are equivalently posed in terms of the temporal evolution of the boundary condition. While a feedforward solution scheme to the inverse integration problem involving computations of correlation/convolution integrals results, for forward integration, a system of integro-differential equations driven by convolution integrals has to be solved. The resulting scheme can be classified as a method of moments, as the impact of the moments into the evolution of the boundary condition is required to complete the system model. The method is illustrated on a batch crystallization process case study. In other applications, the method needs to be adapted accordingly.

Several extensions of the method are of interest, including to the inhomogenous PBE with additional creation/depletion terms, as well as, to the multidimensional PBE with multiple internal coordinates. The proposed approach provides a new framework for future research in optimization and control of PBEs involving size dependent growth kinetics. Using the inverse integration scheme a dynamical optimization problem can be reduced to a static nonlinear program for a given parametrization of the control variable. Alternatively, the introduced modeling formalism provides a suitable testbed for application of semi-analytical optimization techniques such as the minimum principle. Its use in the flatness-based control context seems to be appealing.

Process parameters:
$k_b = 3.4177 \cdot 10^{10} \frac{1}{\mathrm{m}^3 s}$; $b = 2.3463$; $k_g = 1.3718 \cdot 10^{-5} \frac{m}{s}$; $g = 0.7253$ $a_0 = 0.0257$; $a_1 = 1.2 \cdot 10^{-3} \frac{1}{^\circ\mathrm{C}}$; $a_2 = 3.442 \cdot 10^{-5} \frac{1}{^\circ\mathrm{C}^2}$ $\rho = 1250 \frac{\mathrm{kg}}{\mathrm{m}^3}$; $k_v = 0.0288$
C-R model:
$\gamma(\ell) = 1 + \alpha\ell$; $\alpha_1 = 200 \frac{1}{\mathrm{m}}$; $\alpha_2 = 400 \frac{1}{\mathrm{m}}$; $\alpha_3 = 800 \frac{1}{\mathrm{m}}$
Initial conditions:
$f_0(\ell) = \frac{1}{\eta_0} \cdot N(\ell)$; $N(\ell) = \mathcal{N}(\ell; \bar{\mu}_1, \sigma_1^2) + \mathcal{N}(\ell; \bar{\mu}_2, \sigma_2^2))$; $\mathcal{N} \rightarrow$ normal distribution $\bar{\mu}_1 = 8 \cdot 10^{-4}$; $\sigma_1 = 1.7 \cdot 10^{-4}$; $\bar{\mu}_2 = 16 \cdot 10^{-4}$; $\sigma_2 = 2.5 \cdot 10^{-4}$; $\eta_0 = \frac{m_s}{\rho k_v \int_0^\infty \ell^3 N(\ell) \mathrm{d}\ell}$ $m_s = 2.5 \cdot 10^{-3}$kg; $m_w = 0.8017$ kg $m_0 = 0.09915$ kg (simulation); $m_0 = 0.105$ kg (dynamic inversion)

Table 1. Case study table.

ACKNOWLEDGEMENTS

I wish to thank Dr. Shamsul Qamar for many helpful discussions and for sharing his experience with the high resolution finite volume scheme. In particular, I gratefully acknowledge the anonymous reviewer whose comments had a significant impact in the improvement of the manuscript quality.

REFERENCES

Abegg, C.F., Stevens, J.D., and Larson, M.A. (1968). Crystal size distributions in continuous crystallizers when growth rate is size dependent. *AIChE*, 14(118).

Bajcinca, N., Hofmann, S., Raisch, J., and Sundmacher, K. (2010). Robust and optimal control scenarios for batch crystallization processes. *sub. ESCAPE-20.*

Braatz, R.D. (2002). Advanced control of crystallization processes. *Annual Reviews in Control*, 26, 87–99.

Gunawan, R., Fusman, I., and Braatz, R.D. (2004). High resolution algorithms for multidimensional population balance equations. *AIChE Journal*, 50(11), 2738–2749.

Koren, B. (1993). A robust upwind discretisation method for advection, diffusion and source terms. *Numerical Methods for Advection-Diffusion Problems, Ed. C.B.Vreugdenhil and B.Koren, Vieweg, Braunschweig*, p.117.

McGraw, R. (1997). Description of aerosol dynamics by the quadrature method of moments. *Aerosol Science and Technology*, 27, 255–265.

Myerson, A.S. (2002). *Handbook of Industrial Crystallization.* Boston [u.a.] Butterworth-Heinemann.

Qamar, S., Elsner, M.P., Angelov, I., Warnecke, G., and Seidel-Morgenstern, A. (2006). A comparative study of high resolution schemes for solving population balances in crystallization. *Computers and Chemical Engineering*, 30(6-7), 1119–1131.

Ramkrishna, D. (2000). *Population Balances: Theory and Applications to Particulate Systems in Engineering.* Academic Press, A Harcourt Science and Technology Company, second edition.

Randolph, A.D. and Larson, M.A. (1988). *Theory of Particulate Processes.* Academic Press, Inc.

Vollmer, U. and Raisch, J. (2006). Control of batch crystallization - a system inversion approach. *Chem. Eng. Proc.*, 45, 874–885.

Copyright held by the International Federation of Automatic Control